Received: 12 November 2024 | Revised: 3 March 2025 | Accepted: 10 June 2025 | Published online: 29 September 2025

RESEARCH ARTICLE

Journal of Data Science and Intelligent Systems
2025, Vol. 00(0) 1–10
DOI: 10.47852/bonviewJDSIS52024777

Nephrolithiasis Detection and Classification Based on Supervised Machine Learning

BON VIEW PUBLISHING

Ei Phyu Sin Win[1,*]

[1] *Computer Engineering and Information Technology, Mandalay Technological University, Myanmar*

Abstract: In this paper, the author will provide an extensive exploration of the utilization of computed tomography (CT) image processing techniques for the detection of renal calculi. This is one of the most essential topics worldwide to detect the correct location of renal calculi. In the human system, the two kidneys play a crucial role in water purification and recycling. This research involves four steps: Graphic processing with a median filter, segmentation with the Otsu segmentation algorithm, nephrolithiasis detection, and discrete wavelet transform feature extraction and classification. Data from a large number of hospital patients were collected with CT scans, which diagnose renal calculi. This research studies advanced techniques to detect the extent, segment the area, and improve the detection of kidney stones or normal. This analysis helps locate the rocks through pixel analysis. The system also shows many stone patients. Specifically, the system was refined through a dataset of 1,200 X-ray images, a cubic support vector machine achieved 89.3% training accuracy with five-fold cross-validation to avoid overfitting, and an area under the curve close to 0.85, and the receiver operating characteristic curve is close to one. Its outstanding performance on unseen data led to a 90% testing accuracy, demonstrating its robustness using MATLAB and Python IDLE simulator.

Keywords: CT images, image processing techniques, effective stone detection, median filter, stone diseases, DWT feature extraction

1. Introduction

Doctors often use a manual method to check for stones on X-rays, but using 100% automatic methods makes it more efficient and reduces the risk of errors. This study describes a computer vision-based method to detect urinary stone processes [1]. The basic function of renal calculi is to coordinate the balance of solvents in the blood plasma. On one side of the bladder are the pea-shaped kidneys. Stone patients are becoming more frequent around the world, and most people who suffer from Siderite Filament are unaware of it, as it gradually destroys the kidney before symptoms appear [2]. In the past five years, there have been 16,000 research documents published on detecting renal calculi, utilizing various filters from platforms such as Google Scholar and IEEE Xplore [3]. Low contrast and noisy images are being found by applying digital image processing. A computerized system for detecting renal calculi has been developed using pixel-based imaging and data processing strategies. There is a great deal of noise on computed tomography (CT) scans and magnetic resonance imaging, which is favorable to low accuracy [4].

In this research area, discrete wavelet transform (DWT) and support vector machine (SVM) have been shown to be quite accommodating. This survey applied electronic photography to operate CT scans. Image processing includes adding and editing images [5]. But, CT scan pictures often get from low contrast and speckle noise, which pose important appeals. Detecting renal calculi is particularly difficult due to these factors, as speckle noise is a common characteristic of medical images, degrading image quality by reducing contrast and resolution, which diminishes the diagnostic effectiveness of the images [6]. The renal calculi are discovered using ultrasound images and then removed with a surgical process that includes breaking up the stone into minuscule bits that can be passed down the urinary tract [7]. Because kidney mineral has inferior contrast and dapple noise, discovering them is a hard job. This challenge can be overcome by utilizing the right imaging techniques and filtering methods. Ultrasound images frequently exhibit speckle noise, an artifact that standard filters are ineffective at removing [8].

Contrast stretching, a raster image processing technique, is employed to enhance contrast, remove noise, and identify the stone regions in the pre-processed images [9]. By using classification techniques, the accuracy of the resulting predictive model can be assessed, and any misclassifications can be visualized. The prediction of the proper class for all picture points is the main objective of this research. This issue is addressed by applying appropriate imaging techniques and filters. The k-nearest neighbors (KNN) classifier is in this area [10–15].

2. Literature Review

In the use of automated detection systems to identify kidney stones in CT scan images, many survey methods have been examined. In recent years, kidney stones have emerged as a serious problem in the medical community. If not diagnosed promptly, complications can occur, and it may even require surgical intervention to remove. Studies have shown that kidney stone measurements are more accurate and consistent than traditional linear measurements. Moreover, deep learning (DL) algorithms using abdominal CT without contrast may help to identify stones and reduce the burden of manual detection. A series of CT scans can be used to detect stones, including some that cannot be automatically identified in the lungs. After applying image processing techniques to CT scan images, we used a random search algorithm to find the optimal parameter values for the DL model. The model achieved an accuracy of 98.1% [16].

***Corresponding author:** Ei Phyu Sin Win, Computer Engineering and Information Technology, Mandalay Technological University, Myanmar. Email: panthakhin9001@gmail.com

Yildirim et al. [17] pointed out that a total of 500 NCCT images of patients admitted to Fetşıçıken City Hospital in Eraz, Turkey, due to urinary tract stones, were collected. After the experts completed the labeling process, the presence or absence of stones was indicated. If the overfitting troubles are avoided, data augmentation techniques will be applied to the original photos. To train renal calculi detection, we used the XResNet-50 model. The Fastai(v2) library, built on the Pytorch DL framework, was used to train the XResnet-50 model. To adjust the parameters of the XResnet-50 model, the Adam optimizer and cross-entropy loss functions were applied. The model can show the classification locations that the DL model focuses on. According to this article, entering the cross-sectional area at the lower end of the kidney may cause the model to produce inaccurate results. According to research by Ahmad Walid Salehi, sugar is superior to humans in aspects such as perception [16]. Recognition and word recognition. This approach refers to the role of medical imaging in healthcare and medicine: It is gaining more and more importance. The DL methods are as follows:

It has shown promising results in medical image analysis [18].

Morgan B. McCabe describes radiology as a data-intensive field [19]. By using data processing technology in this field, the terrain is very good. Utilizing DL methods to process valuable data in radiological imaging ensures accurate diagnoses and enables high-performance automation in radiology. Foundation networks for classifying and identifying kidney diseases are recommended. The researchers used deep convolutional neural networks (CNNs) to understand these syndromes. Also, the TensorFlow module and inferential methods were used to calculate and identify the diseases category. They achieved 89.79% accuracy. Detection of kidney disease using CNN was used for classification. Chronic kidney disease is 86.67%.

2.1. Digital images

The digital images possess distinct fundamental characteristics, one of which is the image type. For instance, a grayscale image captures only the intensity of light for each pixel, resulting in a range of shades from black to white. In contrast, a color image typically utilizes a combination of colors, often using red, green, and blue (RGB) or cyan, magenta, yellow, and black color models to produce a wide range of hues.

Gray-scale images, also known as monochrome or single-color images, contain only gray-level information, without any color data. The number of different gray levels in these images depends on the number of bits allocated per pixel. For example, an image with 256 gray levels requires 8 bits per pixel, as illustrated in Figure 1. Medical imaging and astronomy often use 12 or 16 bits per pixel for greater detail.

Color images are three separate monochrome image channels, each representing a different. Each color channel contains gray-level information, which is the actual data stored in the digital image. The images containing RGB components are called color images or RGB images. By utilizing the 8-bit monochrome model as a measure, color image characteristics have 24 bits per pixel, with 8 bits allocated to each of the three color bands (RGB), as shown in Figure 2.

Renal calculi imaging is a popular method used to diagnose and plan treatment for renal calculi using different imaging modalities. Renal calculi imaging is important in monitoring the disease after appropriate treatment or surgery [20]. It is designed to identify the location of the stones by creating images of the anatomical structures of the kidney, such as the pelvis and renal stones. Imaging is used to check if the kidneys are functioning properly when choosing the right treatment for renal calculi patients and to understand if the treatment will be successful [21]. Imaging tests serve as a valuable tool for urologists in diagnosing patients who are hospitalized with kidney issues. Additionally, they assist in determining the location and size of renal stones following the initial diagnosis, which is a crucial first step. To access renal calculi, various imaging methods are available.

In order to choose the most suitable method, factors such as cost, ionizing radiation, and the body composition of the imaging device must be considered [22]. Imaging methods can help patients choose the best treatment for renal calculi when compared to other treatment methods such as shock wave lithotripsy, ureteroscopy, or percutaneous shock wave nephrectomy [23].

CT is a scanning method that can produce both enhanced and unenhanced images, and the imaging time varies depending on the clinical situation. CT offers remarkable imaging capacities, giving superior spatial resolution and contrast. These attributes enable urologists to identify kidney abnormalities effectively. CT imaging of the kidneys generates noninvasive cross-sectional views of the organ and is employed in diagnosing a range of conditions, such as renal stones [24].

CT imaging can detect renal calculi and other abnormalities of the urinary system by capturing the full length of the image from the upper kidney to the lower bladder. Reliable imaging of factors such as stone location and size is essential for proper management of renal calculi. Figure 3 shows a stone found in the collecting system of the left kidney of a patient [25].

Figure 1
Example of gray image

Figure 2
Example of a color image

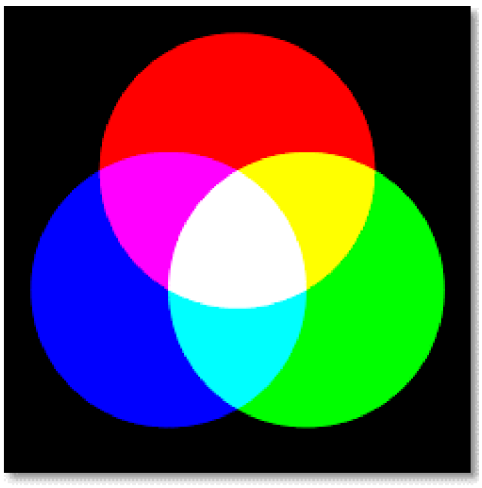

Figure 3
Imaging of renal calculi with non-contrast CT

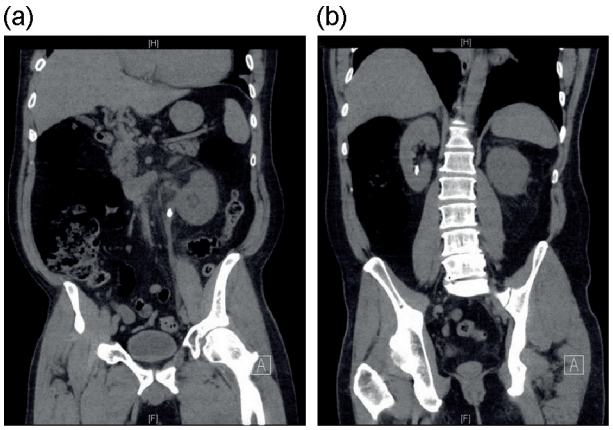

The early step in diagnosis is superior resolution imaging of the abdomen and pelvis. With these images, the presence of renal calculi can be assessed. CT imaging has a 95% success rate in detecting renal calculi [26].

Contrast X-rays should not be used to image renal calculi. Renal calculi have a high radiation absorption rate due to their multicomponent composition, so the images can be easily evaluated. A blockade stone in the left image is shown in Figure 3. An unobstructed stone is seen in the image on the right [27].

Non-contrast axial X-rays are obtained from the upper part of the renal to the pelvic level. These photographs are evaluated along with sagittal and coronal corrections. Calcium-containing renal calculi are clearly visible on non-contrast X-ray scans, whereas uric acid stones are opaque on plain X-rays and can be successfully produced on CT [28].

Radiography pictures can help detect renal calculi and other irregularities. They also provide a good overview of the urinary system by taking pictures of the anterior region from the top of the kidney to the bottom of the bladder. Reliable knowledge of factors such as stone location and stone size is essential for the appropriate treatment of renal calculi disease. It is a mineral discovered in the collecting system of a sick person with a left kidney in Figure 4 [29].

3. Research Methodology

Input data: The system's input consists of a series of CT scans as Figure 4 which can be delineated as 3D colorimetry pictures of the patient. A CT scan can be described as a 3D grayscale image of a patient. A 3D grayscale image is a use of three natural numbers (the place of each picture element) to represent a natural number.

Figure 4
(a) CT scan (without contrast) and (b) Axial CT slices

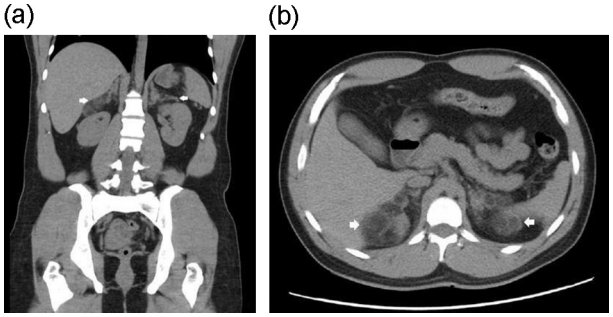

A full CT scan is used as a diagnostic tool, but there are many books around. The SVM algorithm categorizes stone objects. These volumes are chosen by the subsystems previous to the SVM. When training classifiers, it is important to have enough data so that the SVM has enough examples to solve classification and regression tasks. The available data is limited, with only a small number of examples of renal calculi. Image preprocessing step: A collection of methods employed to enhance the image quality and extraction of the essential data from digital images prior to their evaluation using computer vision or machine learning (ML) techniques is included. Several functions, such as processing, filtering, and enlarging the image to make it suitable for further analysis, are applied. Sparkle noise is removed in the preprocessing step, along with removal of unwanted artifacts, abrupt image changes, and image distortion to adjust the high-quality image movement to meet specific processing requirements and reduce the cost of enhancement, or image properties and enhancements that ensure that pixel values are measured accurately. Other methods may include color channel transformation, averaging, pattern operations, or image segmentation, depending on the use case. The use of subsequent image processing methods, computer vision, or ML (e.g., detection, classification, or recognition can be greatly enhanced.

Otsu thresholding is a binarization near that utilizes the use of colorimetry histogram to achieve excellent isolation. The separation result depends on whether there is a large interclass variation (Vb) or a small interclass variation (Vw).

Step 1: The grayscale histogram of an image with an intensity level is defined by Equation 1 as follows:

$$H(i) = \sum_{x=1}^{M} \sum_{y=1}^{N} [I(x, y)] \tag{1}$$

where the width and height of the image are represented with M and N, respectively. The image is represented as I(x, y), where each resolution unit (pixel) at position (x, y) has a value of 1 if the severity at that point meets a specified threshold, and 0 otherwise.

Step 2: To calculate the CDF from the grayscale histogram, we sum the values of each histogram.
The extreme positions are in Equation 2 as follows

$$C(i) = \sum_{j=0}^{i} \frac{H(j)}{M \times N} \tag{2}$$

Step 3: Let μ be the image's mean grayscale intensity value. The mathematical formulation is in Equation 3 as follows:

$$\mu = \frac{1}{M \times N} \sum_{x=1}^{M} \sum_{y=1}^{N} (x, y) \tag{3}$$

Step 4: The user can calculate the mean grayscale intensity values m_0 (T) and m_1(T) as follows in Equations 4 and 5:

$$m_0(T) = \frac{\sum_{i=0}^{T-1} i.H(i)}{P0(T).MN} \tag{4}$$

$$m_1(T) = \frac{\sum_{i=1}^{255} i.H(i)}{P1(T).MN} \tag{5}$$

Step 5: And so, first, the users calculate the between-class variance for each possible threshold value. The best threshold value, denoted as T_{opt}, is then chosen by the threshold value that yields the maximum between-class variance. The users can mathematically show in Equation 6 as follows and Figure 5 shows segmented image:

Figure 5
Example of a segmented image

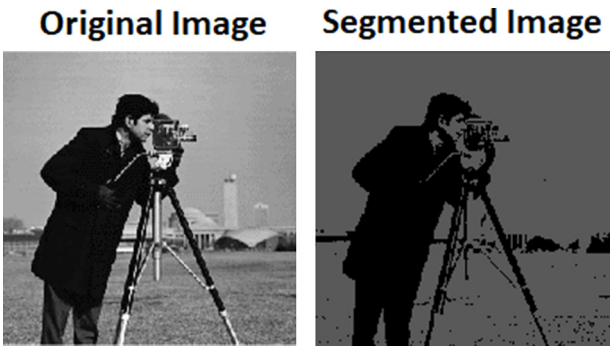

$$T_{\text{opt}} = \text{argmax}\ \ \text{T}\ \ (\text{var}(\text{T})) \tag{6}$$

Here, var(T) represents the between-class variance for a given threshold value, *T*, and argmax T means that the researchers choose the value of *T* that maximizes var(T) in Figure 5.

Image filtering involves modifying the appearance of an image by adjusting the colors of its pixels. This process can enhance contrast or introduce various special effects. A Gaussian noise removing filter is employed in this research. The Gaussian smoothing operator calculates a weighted average of neighboring pixels according to the Gaussian distribution. It is primarily used to reduce Gaussian noise and serves as a realistic model for simulating the effects of a defocused lens. Sigma defines the amount of blurring. The radius slider is used to control how large the template is shown in Figure 6.

2D convolution: To smooth the images, the 2D convolution operator Gaussian filter is applied, and then it removes noise in Figure 7.

The approximation of the continuous Gaussian function designs 2D Gaussian masks. According to the theory, the Gaussian distribution stretches endlessly across all levels, necessitating an enlarged convolution kernel. But in practical applications, the values diminish to a negligible amount beyond roughly three standard deviations from the mean, which permits us to truncate the kernel at that point. An example of an integer-valued convolution kernel is under that closely resembles a Gaussian distribution with a standard deviation of 1.0, as illustrated in Equation 7.

Figure 6
Gaussian filter

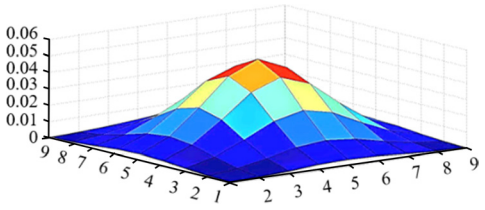

Figure 7
2D convolution operator

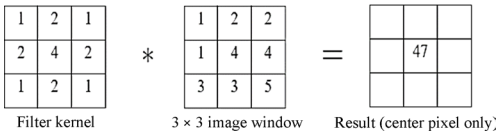

$$\text{G}(\text{x},\text{y}) = \frac{1}{2\pi\sigma^2}\text{e}^{-\frac{\text{x}^2+\text{y}^2}{\sigma^2}} \tag{7}$$

Feature extraction is an important process in image processing and computer vision that focuses on identifying and capturing important structures in an image. This step converts raw image data into digital features that preserve the most important information. Allows for further analysis and simplification.

DWT feature extraction: Any arbitrary function represented as a superposition of wavelets is referred to as a wavelet transform. The activities of dilation and translation are used on a mother wavelet to produce these wavelets. This mathematical technique is useful for decomposing a function into its time and frequency components. For nonstationary signals, it outperforms the classical Fourier transform on the condition of localization, which should be in both the time and frequency domains [30]. The DWT captures both spatial characteristics and frequency information. The DWT breaks down the illustration into a general estimation through low-pass filtering and detailed features through high-pass filtering. This type of decomposition is carried out recursively on low-pass estimation constants produced at each level, until the need number of iterations is achieved. This system utilizes 13 texture measures derived from the co-occurrence matrix. These selected features encompass three categories: contrast, order, and descriptive statistics. The mathematical expressions related to these texture features can be found in Equations 8 to 20 [31].

$$\begin{matrix}\text{Mean}\\ \text{Standard}\end{matrix} = \sum_{\text{m}}^{\text{i}=1}\frac{1}{\text{M}}\text{P}_{\text{ji}} \tag{8}$$

$$\text{Deviation}: \sigma_{\text{j}} = \sqrt{\frac{1}{\text{M}}}\sum_{\text{M}}^{\text{i}=1}\left(\text{P}_{\text{ji}} - \text{M}_{\text{j}}\right)^3 \tag{9}$$

$$\text{Entropy}: \quad -\sum\sum \text{q}(\text{i},\text{j})\ \ \log\ \ \text{q}(\text{i},\text{j}) \tag{10}$$

$$\text{RMS(root mean square)}: \quad \sqrt{\frac{1}{\text{n}}\left(\text{x}_1^2 + \text{x}_2^2 + \cdots + \text{x}_n^2\right)} \tag{11}$$

$$\text{Variance}: \sum_{\text{i}}\sum_{\text{j}}\left(\text{i}-\mu\right)^2 \quad \text{P}\ (\text{i},\text{j}) \tag{12}$$

$$\text{Smoothness}: \qquad \text{Q} = 1 - \frac{1}{1+\sigma^2} \tag{13}$$

$$\text{Kurtosis}: \mu_4 = \sigma^4\ \ \sum_{\text{i}=0}^{\text{G}-1}\left(\text{i}-\mu\right)^4\text{P}(\text{i}) - 3 \tag{14}$$

$$\text{Skewness}\ \mu_3 = \sigma^3\ \ \sum_{i=0}^{G-1}\left(i-\mu\right)^3 P(i) \tag{15}$$

$$\begin{matrix}\text{IDM(Inverse}\\ \text{Difference}\\ \text{Movement)}\end{matrix}: \text{f}_{\text{n}} = \sum_{\text{i}=0}^{\text{N}_{\text{g}}-1}\sum_{\text{j}=0}^{\text{N}_{\text{g}}}\frac{1}{1+(\text{i}-\text{j})^2}\text{P}_{\text{d},0}(\text{i},\text{j}) \tag{16}$$

$$\text{Contrast} = \sum\left(\text{i},\text{j}\right)^2\ \text{q}(\text{i},\text{j}) \tag{17}$$

$$\text{Correlation}: \qquad \sum_{\text{i}=0}^{\text{G}-1}\sum_{\text{j}=0}^{\text{G}-1}[\text{P}(\text{i},\text{j})] \tag{18}$$

$$\text{Energy} = \sum_{j=0}^{G-1}[P(i,j)] \tag{19}$$

$$\text{Homogeneity} = \sum_{i,j}\frac{q\ (j,i)}{1+|j-1|} \tag{20}$$

SVM: The working principle of radial basis function (RBF) SVM is to convert input data into higher-dimensional features. The space intersected by the hyperplane that separates class A Kernel functions, especially RBFs, is used to calculate the similarity between data. A pair of points in this feature space [32].

In RBF SVM, the RBF kernel function is frequently applied.

$$K(x, x') = \exp(-\text{gamma}\ \|x - x'\|) \tag{21}$$

Figure 8
Proposed system design

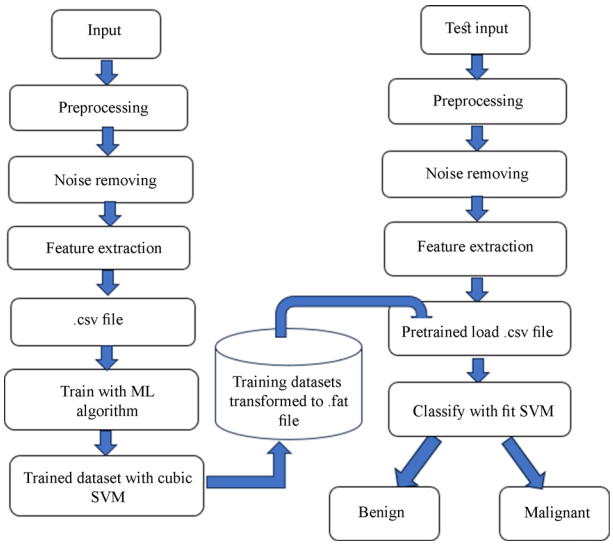

The x and x′ represent single data points in this circumstance.

γ is a hyperparameter that determines the kernel width, and the ‖·‖ symbol represents the Euclidean distance between the data points. In this kernel function, the similarity of data point pairs is evaluated based on the following criteria. Figure 8 describes the proposed system design, and Figure 9 shows the training accuracy percentage with cubic SVM.

The distance within the feature region [33]. Radial basis functions (RBF): In this case, x and x′ are the input data point, gamma γ is a hyperparameter that controls the kernel width, and ‖·‖ represents the Euclidean distance between the points. The kernel function evaluates the similarity between pairs of data points based on the distance between them.

The feature region RBF is used in ML algorithms such as SVMs. When dealing with nonlinear data sets, it can be difficult for users to determine the most appropriate configuration [34].

The Gaussian distribution, which is similar to the RBF kernel, is one of the popular prevalent kernel functions. The RBF kernel function calculates the similarity or proximity of two values, X_1 and X_2, to each other. The confusion matrices and ROC curves of training accuracy are shown in Figures 10 and 11. This kernel can be mathematically represented as follows:

$$K(X_1, X_2) = \exp\left(-\frac{\|X_1, X_2\|^2}{2\sigma^2}\right) \tag{22}$$

where 1. σ is the variance, and our hyperparameter. 2. $\|X_1 - X_2\|$ is the Euclidean (L_2 -norm) distance between two points X_1 and X_2.

The users run the Run.m file, and the Main GUI shown in Figure 12 shows the query image, resized image, histogram image, threshold image, and feature outputs. Figure 13 shows the original image's histogram, and Figure 14 shows after histogram equalization. Figure 15 shows the denoised image of the original image, and Figure 16 shows the message box for the testing result. Figure 17 and Table 1 also show five-time accuracies over Test Image T1. It does not change the result. Table 2 shows that the writer uses the training algorithms such as KKN, Cubic SVM, complex tree, simple tree, logistic regression, Gaussian

Figure 9
Training accuracy

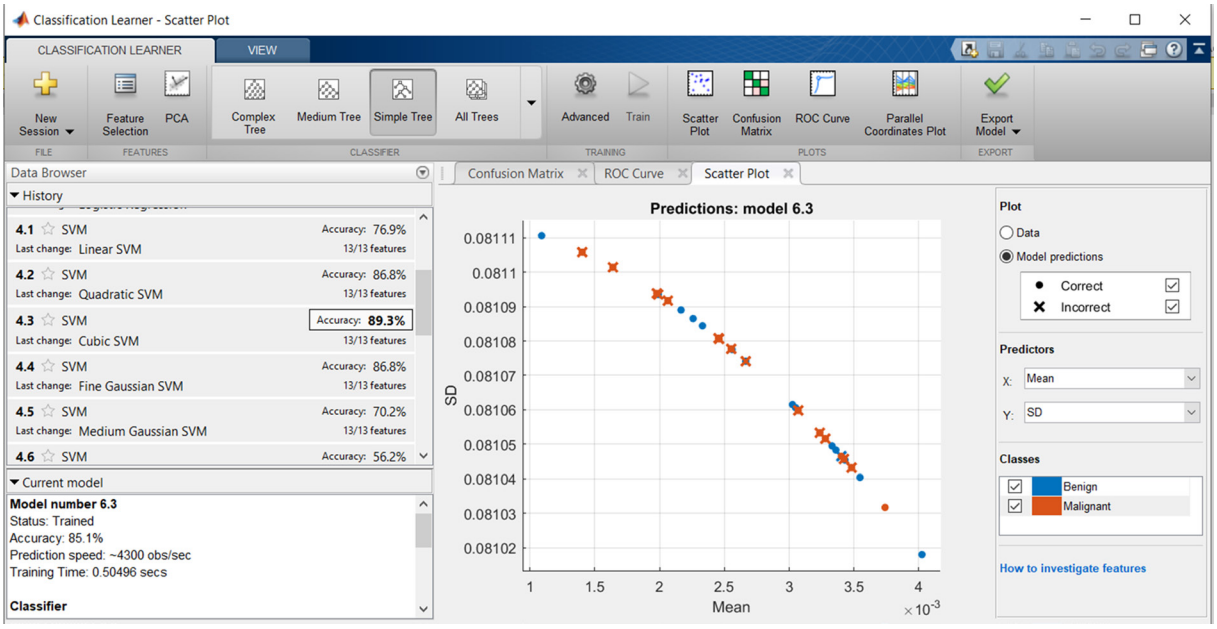

Figure 10
Confusion matrix

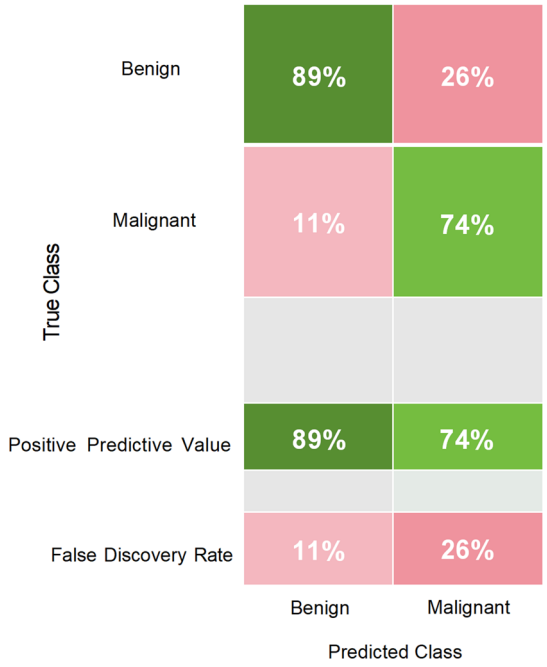

Figure 11
ROC curve

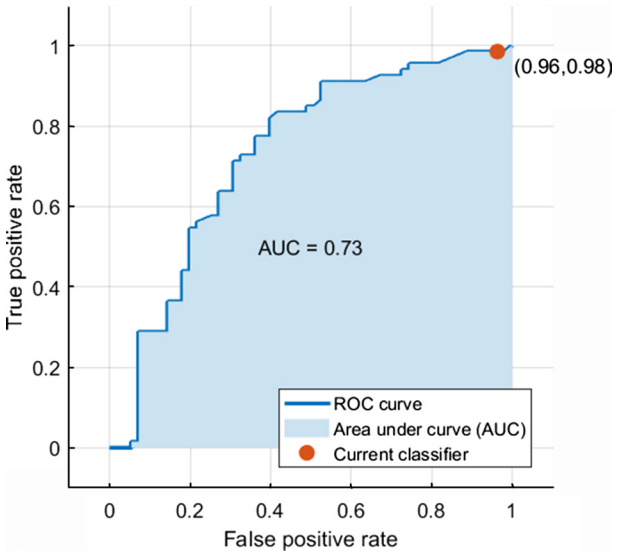

SVM, and ensemble, and Figure 18 also provides accuracy percentages for the training algorithm on the Python Simulator.

3.1. Research design

The system design for kidney stone detection and classification using SVMs involves many theories steps, ranging from data collection and preprocessing to model training and evaluation. An integrated design is shown in Figure 8.

Figure 12
Main GUI

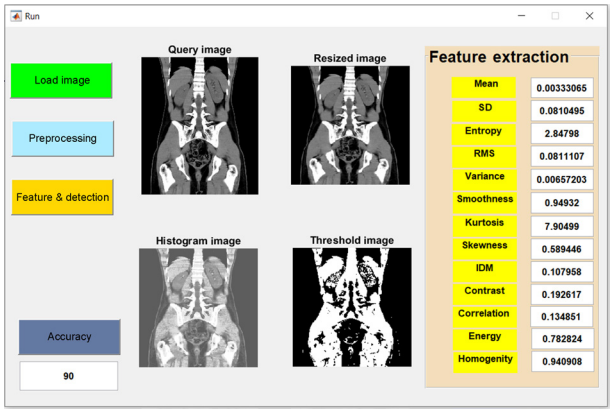

Figure 13
Original image's histogram

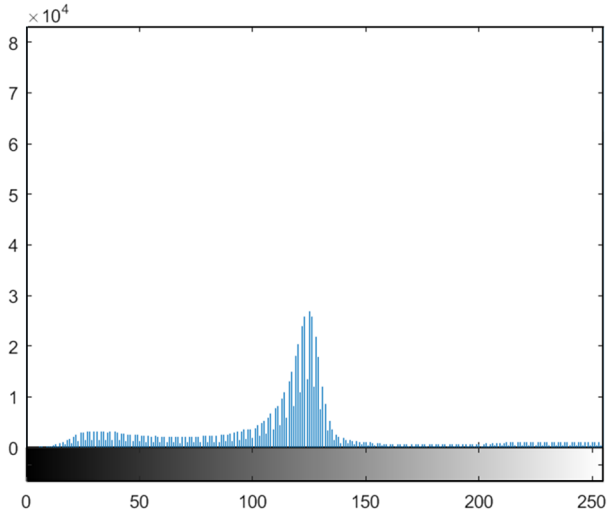

Figure 14
After histogram equalization image's histogram

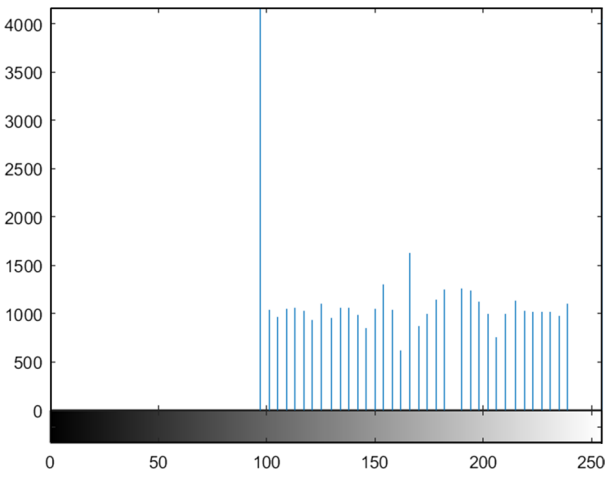

Figure 15
Denoised image using a median filter

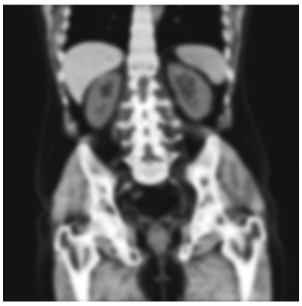

Figure 16
Testing result

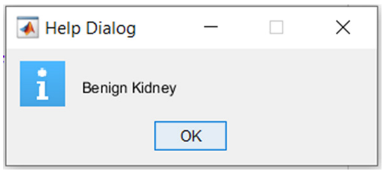

Figure 17
Five-time testing accuracy

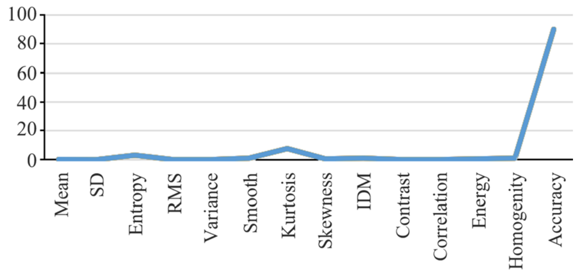

Table 1
Five-time testing accuracy on test image T1

Images	Mean	SD	Entropy	RMS	Variance	Smooth	Kurtosis	Skewness	IDM	Contrast	Correlataion	Energy	Homogenity	Accuracy
T1	0.0026808	0.0810736	3.25142	0.08111	0.00657	0.9378	7.87198	0.64301	0.81935	0.19901	0.98339	0.79339	0.942708	90
	0.0026808	0.0810736	3.25142	0.08111	0.00657	0.9378	7.87198	0.64301	0.81935	0.19901	0.98339	0.79339	0.942708	90
	0.0026808	0.0810736	3.25142	0.08111	0.00657	0.9378	7.87198	0.64301	0.81935	0.19901	0.98339	0.79339	0.942708	90
	0.0026808	0.0810736	3.25142	0.08111	0.00657	0.9378	7.87198	0.64301	0.81935	0.19901	0.98339	0.79339	0.942708	90
	0.0026808	0.0810736	3.25142	0.08111	0.00657	0.9378	7.87198	0.64301	0.81935	0.19901	0.98339	0.79339	0.942708	90

3.2. Requirements

The system necessities are as follows:

▪ Technical (software) necessary

Execution

▪ MS Excel was used to compare accuracy and sensitivity

▪ Technical requirements (hardware)

Customs' duties

Microsoft Windows 10

Minimum requirements: Any Intel or AMD ×86-64 processor.

Recommended: Intel or AMD ×86-64 processor with four cores and AVX2 language setting support

Minimum: 4 GB of HDD space for MATLAB, 5 – 8 GB for a standard installation.

Recommended: SSD is recommended.

Microsoft Windows 10

The required configuration for MATLAB is sufficient to run and edit MS Office.

▪ Higher Intel 8th generation CPU, Small Nvidia 1650 GPU is a necessity for using Classification Learner, cubic SVM algorithm trains 89.3% accuracy.

Table 2
Comparison of the performance of seven shallow ML models according to the 1,200 data types with fold = 5 training

Number	ML Models	Training %	ROC	AUC %	Training time
1	KNN	84.9%	0.79%	0.82%	0.51883 s
2	Cubic SVM	89.3%	0.98%	073%	0.50496 s
3	Complex Tree	55.4%	0.11%	0.75%	0.65935 s
4	Simple tree	80.0%	0.98%	0.73%	2.8542 s
5	Logistic regression	73.6%	0.77%	0.73%	2.7692 s
6	Gaussian SVM	86.8%	0.78%	0.63%	0.57931 s
7	Ensemble	89.3%	0.93%	0.84%	5.4678 s

Figure 18
Comparison bar chart of the performance of seven shallow ML models

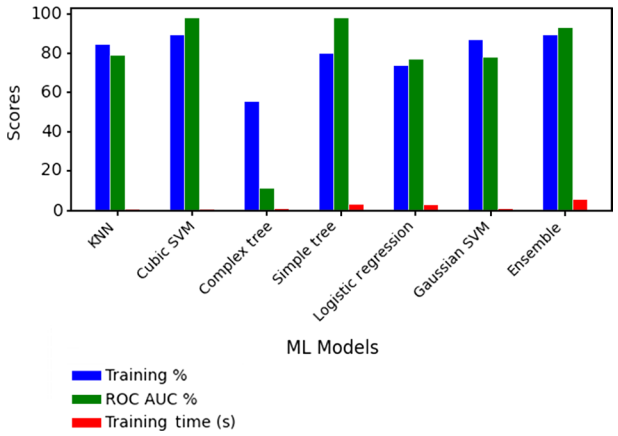

This automatically estimates an optimal threshold value for the image using Otsu's method. Otsu's method is a statistical near to ascertain the threshold that minimizes the intra-class variance, which helps in segmenting the image into viewfinder and background in Axis 4.

3.3. SVM testing accuracy

The table shows the 13 feature parameters' values, and Figure 17 shows the five-time testing accuracy values chart on T1 Image. Table 1. T1 (Benign Kidney) Image Testing Results and Chart.

4. Conclusion

Urolithiasis is a common syndrome affecting about one in 10 humans. Both habitual and general syndromes indicate the degree of consequence of the syndrome, which is the truth. As with any disease, accurate renal calculi examination is essential. A CT scan is a popular imaging method used to examine renal calculi. Especially in identifying renal calculi, interpreting their composition, their space in the renal tubules, size, and number of stones provides important information for the treatment and cure of the disease. A CT scan of the kidney provides accurate access to this information because CT has high sensitivity. From this information about renal calculi, the doctor will determine the appropriate care technique. Information regarding the severity of the condition can be gathered both during and following treatment. Despite the high accuracy of CT scans in identifying renal calculi, radiologists still need to manually examine numerous images to evaluate the condition.

This method can be tedious and time-consuming, as radiologists typically rely on visual assessments of the CT images. Due to manual analysis, human error is possible. In this research, ultrasound pictures cannot be classified.

Further research will explore the development of ML algorithms specifically designed for the classification and analysis of ultrasound images related to urolithiasis. By leveraging large datasets and advanced imaging techniques, these systems aim to enhance diagnostic accuracy and streamline the workflow for radiologists. Additionally, integrating automated ultrasound image classification into clinical practice could facilitate earlier detection and more personalized treatment plans for patients suffering from renal calculi.

Ethical Statement

The data and images presented in this article are sourced from public datasets: Kidney-Stone-Detection, Kidney_stone_detection, and CT KIDNEY DATASET: Normal-Cyst-Tumor and Stone, which are available on GitHub and Kaggle. The author of this article did not directly collect these images.

Conflicts of Interest

The author declares that he has no conflicts of interest to this work.

Data Availability Statement

The data that support the findings of this study are openly available in GitHub at https://github.com/junaid-1013/Kidney-Stone-Detection, https://github.com/muhammedtalo/Kidney_stone_detection, and in Kaggle at https://www.kaggle.com/datasets/nazmul0087/ct-kidney-dataset-normal-cyst-tumor-and-stone.

Author Contribution Statement

Ei Phyu Sin Win: Conceptualization, Methodology, Software, Validation, Formal analysis, Investigation, Resources, Data curation, Writing – original draft, Writing – review & editing, Visualization, Supervision, Project administration.

References

[1] Baygin, M., Yaman, O., Barua, P. D., Dogan, S., Tuncer, T., & Acharya, U. R. (2022). Exemplar Darknet19 feature generation technique for automated renal calculi detection with coronal CT images. *Artificial Intelligence in Medicine*, *127*, 102274. https://doi.org/10.1016/j.artmed.2022.102274

[2] Lopez-Tiro, F., Estrade, V., Hubert, J., Flores-Araiza, D., Gonzalez-Mendoza, M., Ochoa, G., & Daul, C. (2024). On the in vivo recognition of kidney stones using machine learning. *IEEE Access*, *12*, 10736–10759. https://doi.org/10.1109/ACCESS.2024.3351178

[3] Yılmaz, Ü., İnci, A., Özcan, E., Gül, S., Berber, H. G., Eşkin, F. P., ... & Çekin, A. H. (2022). Gallbladder stone prevalence and related factors in predialysis chronic kidney disease patients. *The Turkish Journal of Gastroenterology*, *33*(9), 760–766. https://doi.org/10.5152/tjg.2022.22350

[4] Saini, R. K., Saini, H., & Singh, H. (2024). Enhanced kidney stone detections using digital image processing techniques. *SN Computer Science*, *5*(6), 790. https://doi.org/10.1007/s42979-024-03133-4

[5] Singh, S. P., Praveena, S., & Suresh Kumar, B. (2022). Kidney stone detection from CT scan using CNN. *International Journal of Innovative Research in Science, Engineering and Technology*, *11*(6), 1–8.

[6] Kumar, A., Pandey, S. K., Varshney, N., Singh, K. U., Singh, T., & Shah, M. A. (2023) Distinctive approach in brain tumor detection and feature extraction using biologically inspired DWT method and SVM. *Scientific Reports*, *13*, 22735. https://doi.org/10.1038/s41598-023-50073-9

[7] Paka, N. R., Guggalashettara, B., Ankitha, H. K., & Archana, K. (2024). Kidney stone detection and stone analysis using image processing. *International Journal for Research in Applied Science and Engineering Technology*, *12*(5), 3977–3982. https://doi.org/10.22214/ijraset.2024.62433

[8] Zhang, S. (2021). Challenges in KNN Classification. *IEEE Transactions on Knowledge and Data Engineering*, *33*(2), 1234–1245. https://doi.org/10.1109/TKDE.2021.3049250

[9] Kaur, G., & Singh, S. (2022). Image quality enhancement and noise reduction in kidney ultrasound images. *International Journal for Research in Applied Science and Engineering Technology*, *10*(7). 2321–9653. https://doi.org/10.22214/ijraset.2022.45490

[10] Nazmdeh, V., & Esmili, S. S. (2022). A review of methods for detection and segmentation of kidney stones from CT scan images using image processing method. *International Journal of Cybernetics and Cyber-Physical Systems*, *1*(2), 157–168. https://doi.org/10.1504/IJCCPS.2022.124877

[11] Chen, X., & Cheng, Q. (2024). Acute complication prediction and diagnosis model CLSTM-BPR: A fusion method of time series deep learning and Bayesian personalized ranking. *Tsinghua Science and Technology*, *29*(5), 1509–1523. https://doi.org/10.26599/TST.2023.9010103

[12] Lu, K., Wang, H., Wang, W., & Kudo, M. (2020). VHP: Approximate nearest neighbor search via virtual hypersphere partitioning. *Proceedings of the VLDB Endowment*, *13*(9), 1443–1455. https://doi.org/10.14778/3397230.3397240

[13] Ozturk Kiyak, E., Ghasemkhani, B., & Birant, D. (2023). High-level K-nearest Neighbors (HLKNN): A supervised machine learning model for classification analysis. *Electronics*, *12*(18), 3828. https://doi.org/10.3390/electronics12183828

[14] Beskopylny, A. N., Stel'makh, S. A., Shcherban', E. M., Mailyan, L. R., Meskhi, B., Razveeva, I., ... & Beskopylny, N. (2022). Concrete strength prediction using machine learning methods CatBoost, k-nearest neighbors, support vector regression. *Applied Sciences*, *12*(21), 10864. https://doi.org/10.3390/app122110864

[15] Lu, J., Qian, W., Li, S., & Cui, R. (2021). Enhanced K-nearest neighbor for intelligent fault diagnosis of rotating machinery. *Applied Sciences*, *11*(3), 919. https://doi.org/10.3390/app11030919

[16] Vasanthselvakumar, R., Balasubramanian, M., & Sathiya, S. (2020). Automatic detection and classification of chronic kidney diseases using CNN architecture. In *Data Engineering and Communication Technology: Proceedings of 3rd ICDECT-2K19* (pp. 735–744). Springer Singapore. https://doi.org/10.1007/978-981-15-1097-7_62

[17] Yildirim, K., Bozdag, P. G., Talo, M., Yildirim, O., Karabatak, M., & Acharya, U. R. (2021). Deep learning model for automated kidney stone detection using coronal CT images. *Computers in Biology and Medicine*, *135*, 104569. https://doi.org/10.1016/j.compbiomed.2021.104569

[18] Salehi, A. W., Khan, S., Gupta, G., Alabduallah, B. I., Almjally, A., Alsolai, H., ... & Mellit, A. (2023). A study of CNN and transfer learning in medical imaging: Advantages, challenges, future scope. *Sustainability*, *15*(7), 5930. https://doi.org/10.3390/su15075930

[19] Muksimova, S., Umirzakova, S., Kang, S., & Im Cho, Y. (2024). CerviLearnNet: Advancing cervical cancer diagnosis with reinforcement learning-enhanced convolutional networks. *Heliyon*, *10*(9). https://doi.org/10.1016/j.heliyon.2024.e29913

[20] Akram, M., Jahrreiss, V., Skolarikos, A., Geraghty, R., Tzelves, L., Emilliani, E., ... & Somani, B. K. (2024). Urological guidelines for kidney stones: Overview and comprehensive update. *Journal of Clinical Medicine*, *13*(4), 1114. https://doi.org/10.3390/jcm13041114

[21] Jebir, R. M., & Mustafa, Y. F. (2024). Kidney stones: natural remedies and lifestyle modifications to alleviate their burden. *International Urology and Nephrology*, *56*(3), 1025–1033. https://doi.org/10.1007/s11255-023-03764-1

[22] Cheraghian, B., Meysam, A., Hashemi, S. J., Hosseini, S. A., Malehi, A. S., Khazaeli, D., & Rahimi, Z. (2024). Kidney stones and dietary intake in adults: A population-based study in southwest Iran. *BMC Public Health*, *24*(1), 955. https://doi.org/10.1186/s12889-024-18393-1

[23] Ahmed, F., Abbas, S., Athar, A., Shahzad, T., Khan, W. A., Alharbi, M., ... & Ahmed, A. (2024). Identification of kidney stones in KUB X-ray images using VGG16 empowered with explainable artificial intelligence. *Scientific Reports*, *14*(1), 6173. https://doi.org/10.1038/s41598-024-56478-4

[24] Beeharry, Y., & Bassoo, V. (2020). Performance of ANN and AlexNet for weed detection using UAV-based images. In *2020 3rd International Conference on Emerging Trends in Electrical, Electronic and Communications Engineering (ELECOM)* (pp. 163–167). IEEE. https://doi.org/10.1109/ELECOM49001.2020.9296994

[25] Brisbane, W., Bailey, M. R., & Sorensen, M. D. (2016). An overview of kidney stone imaging techniques. *Nature Reviews Urology*, *13*(11), 654–662. https://doi.org/10.1038/nrurol.2016.154

[26] Liu, H., & Ghadimi, N. (2024). Hybrid convolutional neural network and Flexible Dwarf Mongoose Optimization Algorithm for strong kidney stone diagnosis. *Biomedical Signal Processing and Control*, *91*, 106024. https://doi.org/10.1016/j.bspc.2024.106024

[27] Muksimova, S., Umirzakova, S., Mardieva, S., & Cho, Y. I. (2023). Enhancing medical image denoising with innovative teacher–student model-based approaches for precision diagnostics. *Sensors*, *23*(23), 9502. https://doi.org/10.3390/s23239502

[28] Mardieva, S., Ahmad, S., Umirzakova, S., Rasool, M. A., & Whangbo, T. K. (2024). Lightweight image super-resolution for IoT devices using deep residual feature distillation network. *Knowledge-Based Systems*, *285*, 111343. https://doi.org/10.1016/j.knosys.2023.111343

[29] Dangle, P., Tasian, G. E., Chu, D. I., Shannon, R., Spiardi, R., Xiang, A. H., ... & Ellison, J. S. (2024). A systematic scoping review of comparative effectiveness studies in kidney stone disease. *Urology*, *183*, 3–10. https://doi.org/10.1016/j.urology.2023.08.042

[30] Umirzakova, S., Ahmad, S., Mardieva, S., Muksimova, S., & Whangbo, T. K. (2023). Deep learning-driven diagnosis: A multi-task approach for segmenting stroke and Bell's palsy. *Pattern Recognition*, *144*, 109866. https://doi.org/10.1016/j.patcog.2023.109866

[31] Khamparia, A., Singh, P. K., Rani, P., Samanta, D., Khanna, A., & Bhushan, B. (2021). An internet of health things-driven deep learning framework for detection and classification of skin cancer using transfer learning. *Transactions on Emerging Telecommu-*

nications Technologies, *32*(7), e3963. https://doi.org/10.1002/ett.3963

[32] Pan, W., Yun, T., Ouyang, X., Ruan, Z., Zhang, T., An, Y., ... & Zhu, P. (2024). A blood-based multi-omic landscape for the molecular characterization of kidney stone disease. *Molecular Omics*, *20*(5), 322–332. https://doi.org/10.1039/D3MO00261F

[33] Zhang, M., Ye, Z., Yuan, E., Lv, X., Zhang, Y., Tan, Y., ... & Li, Z. (2024). Imaging-based deep learning in kidney diseases: Recent progress and future prospects. *Insights into Imaging*, *15*(1), 50. https://doi.org/10.1186/s13244-024-01636-5

[34] Sudharson, S., & Kokil, P. (2021). Computer-aided diagnosis system for the classification of multi-class kidney abnormalities in the noisy ultrasound images. *Computer Methods and Programs in Biomedicine*, *205*, 106071. https://doi.org/10.1016/j.cmpb.2021.106071

How to Cite: Sin Win, E. P. (2025). Nephrolithiasis Detection and Classification Based on Supervised Machine Learning. *Journal of Data Science and Intelligent Systems*. https://doi.org/10.47852/bonviewJDSIS52024777